Chapter 5. Impedance spectroscopy and electric modulus behavior of Molybdenum doped Cobalt Zinc ferrite

5.1 Introduction

Lately, ferrite materials assume a vital part in present day innovation because of their amazing magnetic, electrical and magneto-electric behaviors. This material has an extensive variety of utilization in different fields like microwave gadgets, magnetic sensors, spintronics, waveguides and transducer and so forth [74, 75, 78, 81, 199]. A few ferrites display multiferroic behavior, make the materials in fact more significant [210]. There are both ferroelectric and ferromagnetic property in multiferroic materials, in a solitary stage [196]. Because of this intriguing conduct, the materials are utilized to construct high-density memory device where the information can be composed and perused in both ways i.e. electrically and magnetically separately and the other way around [66, 197].

Cobalt-Zinc ferrite is a feeble multiferroic material and furthermore have great electrical and magnetic properties [66]. It has inverse spinel structure having *Fd3m* space group. Then common chemical formula of Co-Zn ferrite is $Co_{1-x}Zn_xFe_2O_4$, which can be depicted as $[Fe_{1-x}^{3+}Zn_x^{2+}]^A[Co_{1-x}^{2+}Fe_{1+x}^{3+}]^BO_4$, where 'A' speaks to the tetrahedral site, 'B' speaks to the octahedral site and 'x' portrays the degrees of reversal. Zn-ions want to be at 'A' site while Co-ions occupied in 'B' site and Fe-ions are conveyed between the two

destinations. There is some loss of Zn ions at the time of synthesis and calcination method, which create a cation vacancies and unsaturated Oxygen ions. Extra electrons on Oxygen will bind with the neighboring Fe^{3+} ions, which prompt making Fe^{2+} ions. Along these lines, there is a high likelihood of electron jumping in B-site inside the ferrite [64]. Co-Zn ferrite has some fascinating behaviors for example, high impedance, large magneto-crystalline anisotropy, high coercivity, moderate saturation magnetization, low eddy current, high dielectric constant, minimal effort of assembling and so forth. Because of these superb properties, they have immense applications in high-frequency device, satellite communication, ferrofluids, antenna cores, magnetic switches, biosensor, chemical drug delivery, transformer cores, read/write head of high-speed digital tapes, magneto-caloric refrigeration, photocatalysis, gas sensor and so forth. [207, 215-218].

Such a significant number of researchers have contemplated the dielectric and electrical behaviors, impedance spectroscopy and electrical modulus property of various ferrites with various substituents. Hasim *et al.* [67] examined the impedance spectroscopy of Co-Cu ferrite. Electric modulus investigation gives the data about the nature of the polycrystalline sample and portrays the electrical relaxation in ionic solids. Arjumanara *et al.* [98] explored the electric modulus of Co-Cu-Zn ferrite thoroughly. The detailed dielectric behaviors, impedance spectroscopy and ac conductivity of Ni-Zn ferrite have been contemplated by Mandal *et al.* [61]. Farea *et al.* revealed the electrical behaviors and impedance spectroscopy of Cd substituted Cobalt ferrite [63].

In this chapter, we showed the investigation of impedance spectroscopy and electrical modulus behavior of Mo doped Co-Zn ferrite. The frequency reliance of real and imaginary

part of both complex impedance and electric modulus has been investigated. The activation energy of each sample is ascertained utilizing the Arrhenius law.

5.2 Complex impedance spectroscopy

Complex impedance spectroscopy is a capable procedure which is broadly utilized to describe the electrical features of electroceramic materials, for example, relaxation process, dielectric behavior and electrical conductivity and so on. This strategy empowers one to comprehend the bulk effect and interfaces in the temperature and frequency region [64].

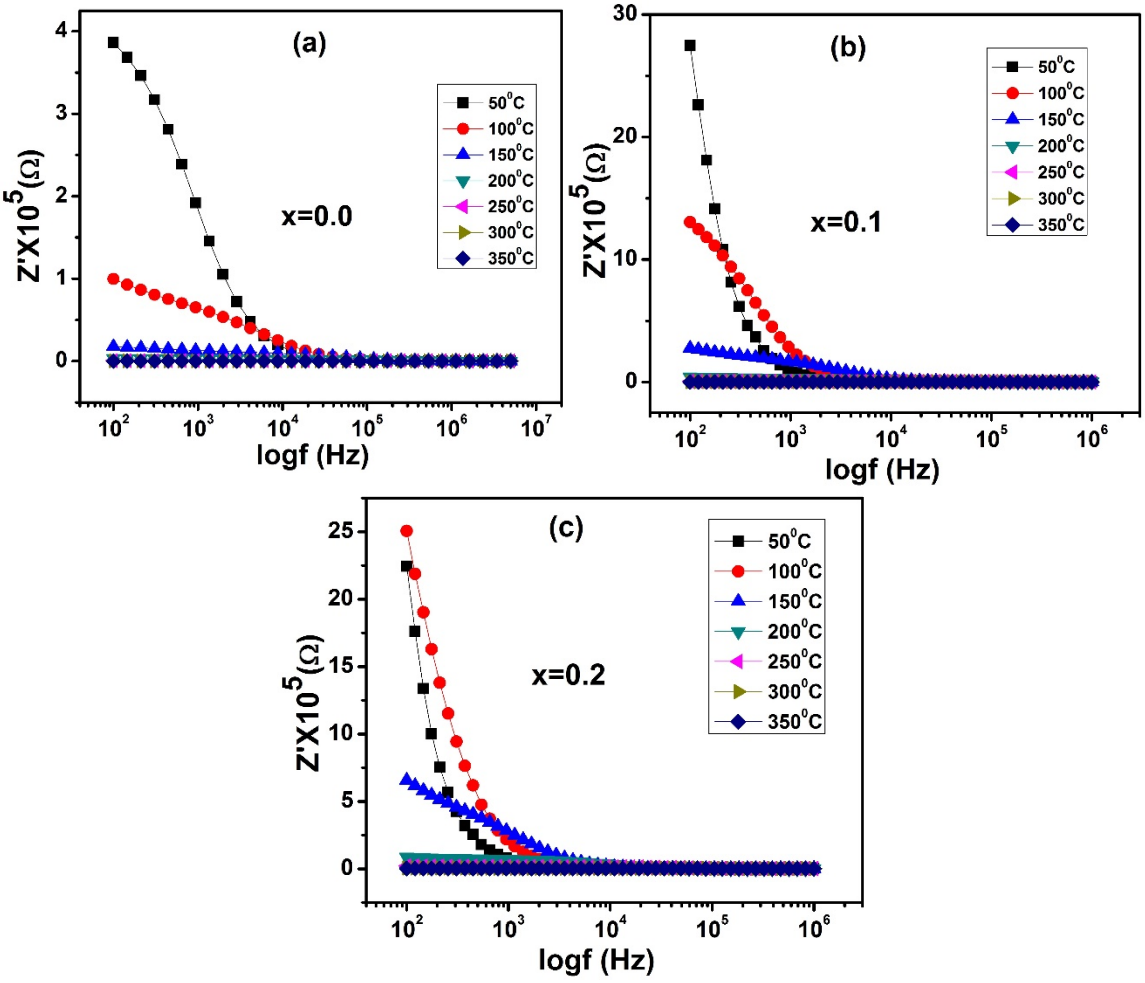

Fig. 5.1. Variation of real part of complex impedance with frequency for different doping concentration of Mo.

Fig. 5.1(a)-(c) depicts the variation of the real part of impedance (Z') with frequency at various temperature for CZMO (x=0.0, 0.1). It was observed that the value of Z' diminishes with increment in frequency and at high frequency all the Z' curves are seen to be combine and turn out to be relatively free of frequency. This might be because of the lessening of space charge polarization at higher frequency [61]. It was also observed that at a specific frequency the impedance diminishes with increment in temperature which propose that the conduction process in the CZMO is because of thermally activated conduction process.

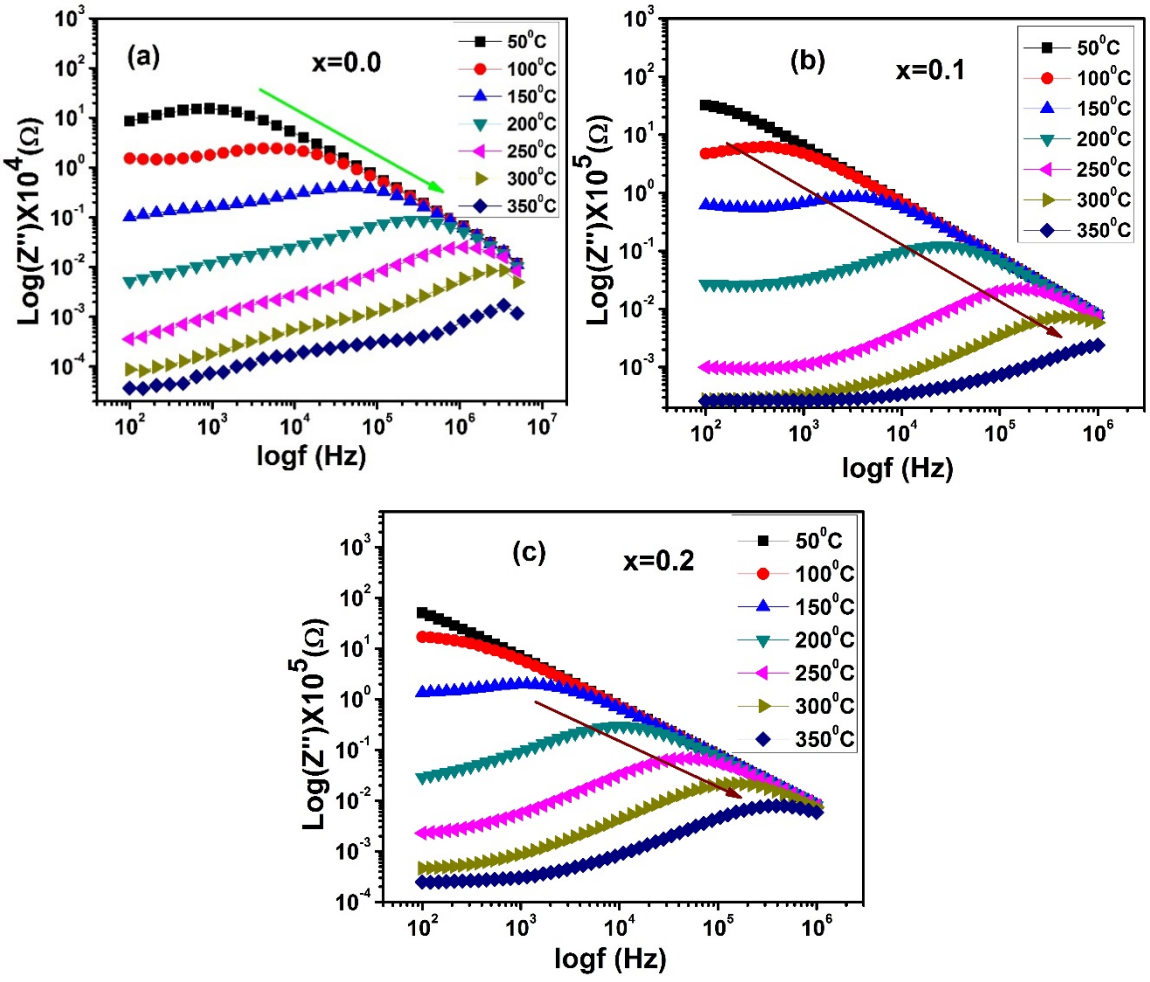

Fig. 5.2. The variation of imaginary part complex impedance with frequency for (a) x=0.0, (b) x=0.1 and (c) x=0.2. The arrow shows the shifting of Z''.

The variation of Z'' with frequency is displayed in Fig. 5.2(a)-(c) for every one of the samples at various temperatures. We have noticed a broad Debye peak for each Z'' vs.f plots at a specific frequency, known as the relaxation frequency(f_0). It is apparent that the peaks are seen to move to the high frequency with increment in temperature. This wonder can be clarified in light of increment in hopping rate of electron at higher temperature. Accordingly, the hopping electrons have less relaxation time and the polarization is decreased at higher frequency [219]. The above perceptions are in great concurrence with the prior perception by Chen et al. for unadulterated Cobalt ferrite [220].

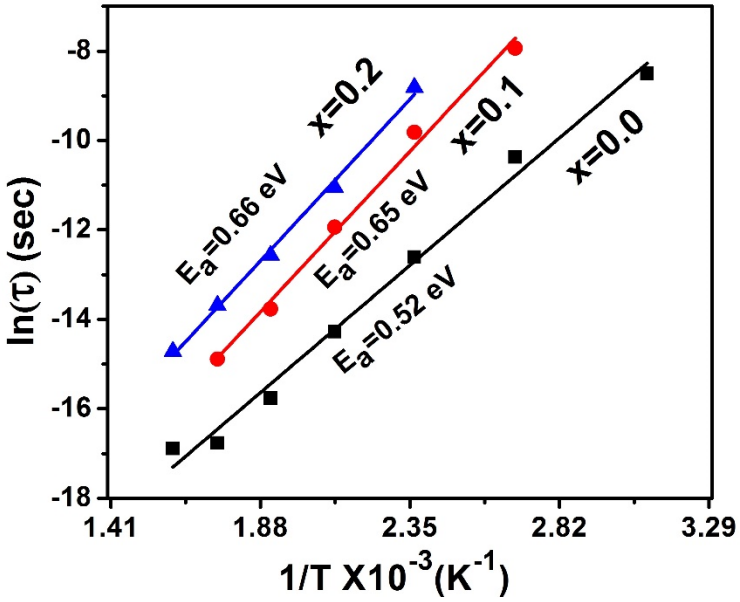

Fig. 5.3. Arrhenius plot and activation energy of CZMO with different Mo doping concentration obtained from impedance data.

In order to calculate the activation energy one should initially figure the relaxation time from Z'' vs.f plot (Fig. 5.2(a)-(c)) utilizing the accompanying condition as

$$\tau = \frac{1}{2\pi f_0} \qquad (5.1)$$

where f_0 is the frequency associate to $Z"_{max}$. Henceforth the activation energy can be estimated for every samples using the Arrhenius condition as

$$\tau = \tau_0 e^{-E_a/k_B T} \qquad (5.2)$$

where τ_0 is the pre-exponential factor, E_a represents the activation energy, the Boltzmann constant is k_B is and T display the absolute temperature. Fig. 5.3 demonstrate the plot of ln τ vs. $\frac{1}{T}$ and from the incline of the straight line acquired one can assess the the activation energy. The ascertained activation energy of CZMO with x=0.0, 0.1, 0.2 are 0.52 eV, 0.65 eV and 0.66 eV respectively. It would seem that the activation energy marginally increases with increment in Mo content.

To comprehend the entire conduction mechanism one ought to acquire the Cole-Cole plot or the Nyquist plot of complex impedance by plotting Z′ vs. Z″. As indicated by Cole-Cole, the dispersion can be clarified based on two layer model. The Nyquist plot by and large comprises of two semi-circular arc. The semi-circular arc at lower frequency side is direct result of grain boundary commitment and the semi-circular arc at the higher frequency side is a result of grain commitment. The nature of the Nyquist plot likewise relies on the grain size. One semi-circular arc may observed for the material with smaller grain size while that with bigger grain size displays two semi-circular arcs [221].

The Nyquist plot, i.e., the real part (Z') vs. the imaginary part ($Z"$) of complex impedance at various temperature for each samples (x=0.0, 0.1, 0.2) are illustrated in Fig. 5.4(a)-(c). In the current sample there is one noticeable semi-circular arc showing the grain

boundary conduction commands over the grain conduction [67]. The Cole-Cole plot of CZMO (x=0.1) at 100ºC is appeared in Fig. 5.4(d), where the solid line speaks to the fitted curve which is very coordinated with the collected impedance data. The noticed Nyquist plot may be spoken to by an equivalent electrical circuit which is appeared in inset of Fig. 5.4(d).

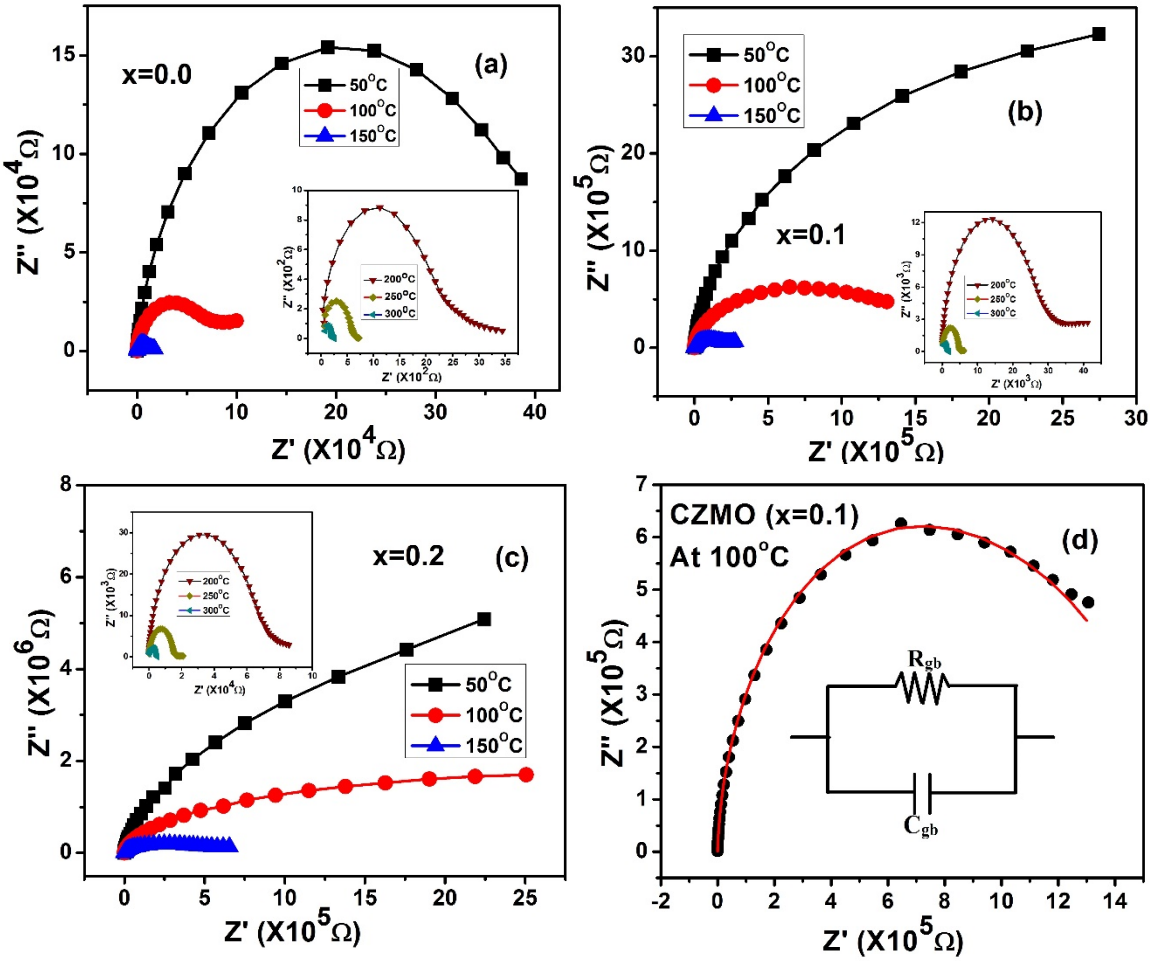

Fig. 5.4. Nyquist plots of complex impedance for (a) x=0.0, (b) x=0.1 and (c) x=0.2 at different temperatures. (d) The Nyquist plot of CZMO (x=0.1) at 100^{O}C and inset shows the electrical equivalent circuit of the sample.

The equivalent circuit comprises of parallel combinations of a resistance and a capacitance. Hence the complex impedance may be expressed by [222, 223]

$$Z^* = Z' + iZ'' \qquad (5.3)$$

Where $$Z' = \frac{R_g}{1+(\omega R_g C_g)^2} + \frac{R_{gb}}{1+(\omega R_{gb} C_{gb})^2} \qquad (5.4)$$

and $$Z'' = \frac{\omega R_g^2 C_g}{1+(\omega R_g C_g)^2} + \frac{\omega R_{gb}^2 C_{gb}}{1+(\omega R_{gb} C_{gb})^2} \qquad (5.5)$$

where R_g and R_{gb} are the grain and grain boundary resistance, respectively. C_g and C_{gb} are the grain and grain boundary capacitance, respectively and the angular frequency is ω. For the most part, the resistance and capacitance and therefore the time constant is bigger for grain boundary in contrast to the grain.

Besides, it is obvious that there is some despondency in each semi-circular arcs and the center of all the semi-circle lies little underneath the abscissa axis suggests the existence of non-Debye type relaxation process in the present sample [224].

5.3 Electric modulus formalism

The complex modulus formalism initially has been presented by P. B.Macedo *et al.* [156][28] to study and inspect the space charge relaxation phenomena, hopping rate of carrier etc. The principle preferred standpoint of this portrayal is that the little capacitance value is much commanding and the impact of electrode polarization is stifled here. The electric modulus may be assessed by utilizing the equation as [157]

$$M^* = M' + iM'' = i\omega C_0 Z^* \qquad (5.6)$$

where, $$C_0 = \frac{\varepsilon_0 A}{d} \qquad (5.7)$$

where ε_0 is the permittivity in free space, A is the area and d is thickness of sample.

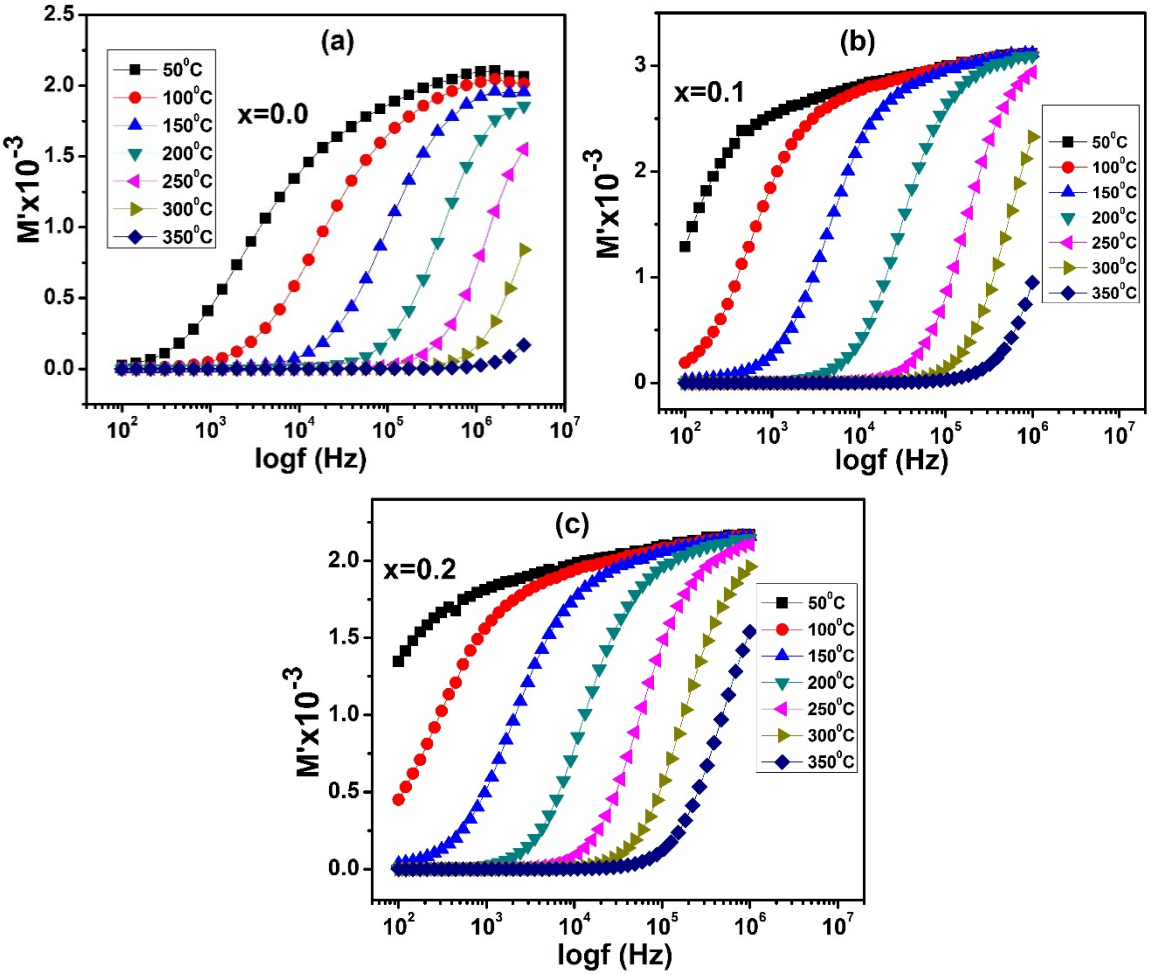

Fig. 5.5. The variation of real part of electric modulus with frequency for different doping concentration of Mo at different temperature.

Fig. 5.5 shows the variation of real part of the electric modulus (M') with frequency at various temperatures. It is noticed that there is a little estimation of M' at low frequency

domain and a constant dispersion with the expansion of frequency and tending to immerse at an asymptotic maximum in the high frequency domain for every samples.

The frequency reliance of imaginary part of the electric modulus (M'') is depicted in Fig. 5.6 for x=0.0, 0.1 and 0.2 at various temperatures. M'' is basically associated with the energy dissipation in the irreversible conduction process. The low frequency tail of the peak illustrates the span of frequencies in which the ions can travel over a long distance,

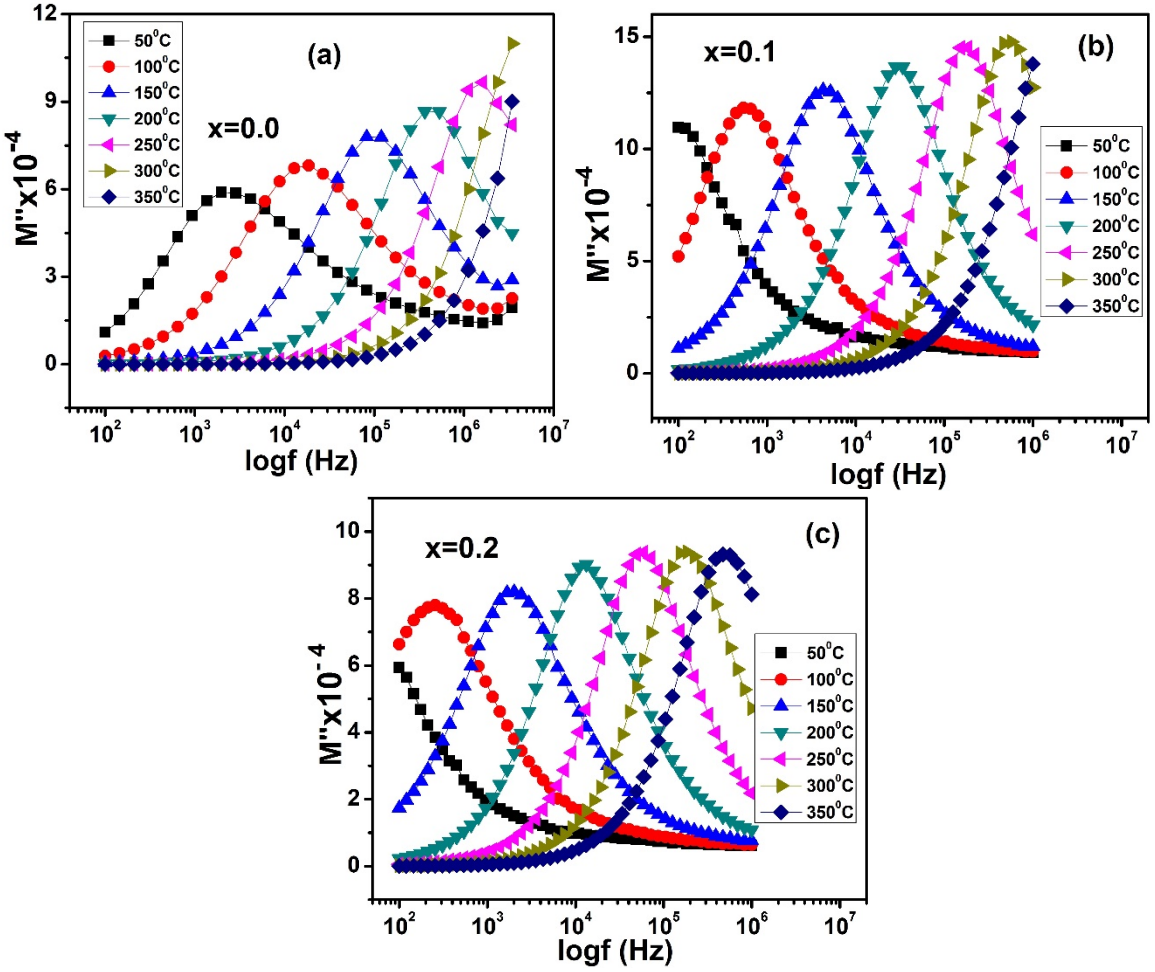

Fig. 5.6. Variation of imaginary part of electric modulus as a function frequency for CZMO with (a) x=0.0, (b) x=0.1 and (c) x=0.2.

results a effective hopping of ions from one site to the adjacent site in the crystal. Whereas the high frequency tail of the M'' peak illustrates the span of frequencies in which the ions are spatially confined in the potential well and capable to make only the localized movement within the well [57]. The M'' peaks signifies the transition from long-range to short-range mobility of the charge carrier at various temperatures.

In our current framework, the electric modulus properties may be articulated by the altered Kohlrausch-Williums-Watts (KWW) function proposed by Bergman [160]. The imaginary part of the electric modulus (M'') is characterized as [161]

$$M'' = \frac{M''_{max}}{(1-\beta)+\frac{\beta}{1+\beta}\left[\beta\left(\frac{fmax}{f}\right)+\left(\frac{fmax}{f}\right)^{\beta}\right]} \tag{5.8}$$

where β called the stretched exponent parameter and f_{max} represents the frequency at M''_{max}. The estimation of β lies in the scope of $0 < \beta \leq 1$. In the present framework, because of the non-Debye type relaxation mechanism the estimation of β is under 1.

In contrast to the Nyquist plot of complex impedance, the complex modulus spectrum can well determine the respective relaxation phenomenon. Fig. 5.7 displays the complex spectrum (M' vs. M'') of CZMO. One semi-circular arc indicate that, the relaxation is because of the grain boundary commitment only and the contribution of grain effect is quenched. The center of the semi-circular arc lies little under the real axis suggesting the non-Debye type relaxation mechanism presents in the CZMO samples which is in great understanding of our prior decisions.

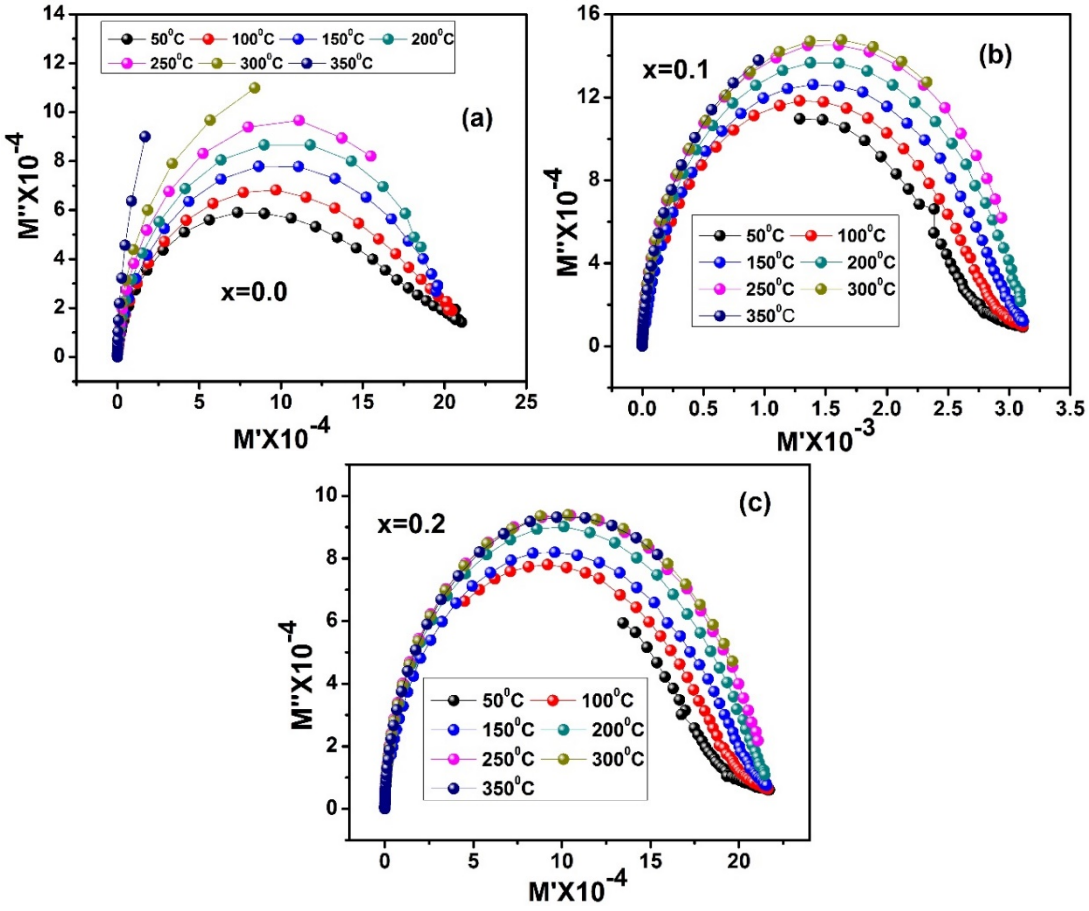

Fig. 5.7. Complex electric modulus spectrum of CZMO {(a) x=0.0, (b) x=0.1 and (c) x=0.2} ferrite.

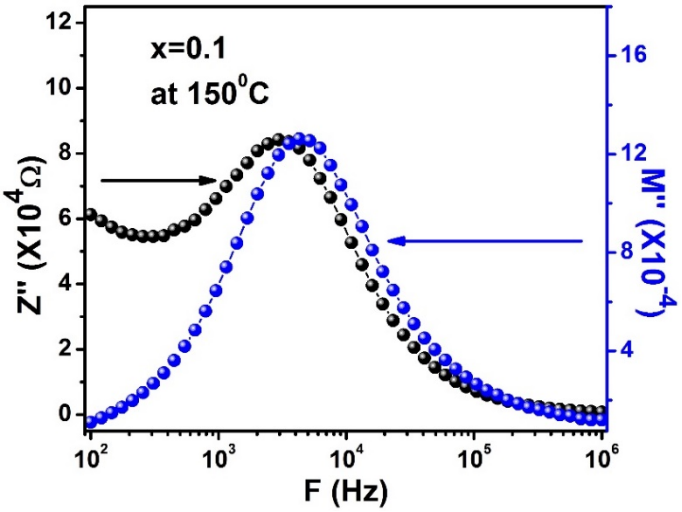

Fig. 5.8. Frequency variation of both impedance and electric modulus for x=0.1 at 150^{O}C.

Fig. 5.8 demonstrates a conventional plot of Z'' and M'' as a function of frequency at 100°C for x=0.1. There is a small separation is noticed between the two peaks related to Z'' and M''. In the perfect Debye type relaxation mechanism the two peaks ought to match with each other at a specific frequency [98]. Be that as it may, in the present case they don't correspond with each other affirming the non-Debye type nature.

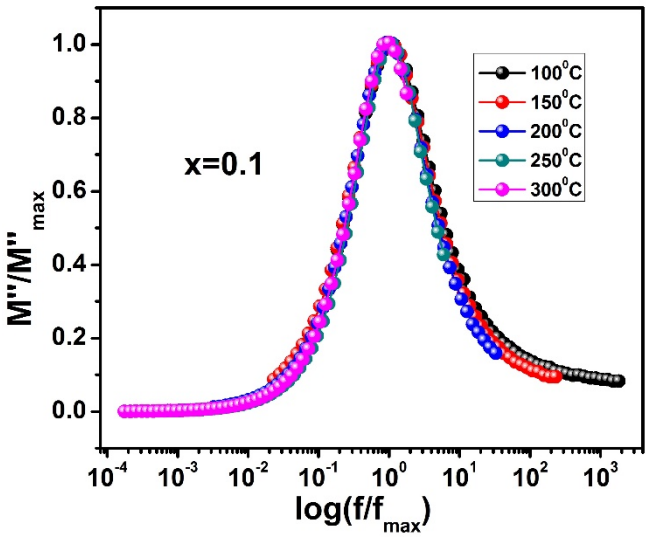

Fig. 5.9. Scaling behavior of electric modulus of CZMO ferrite.

The scaling of modulus spectrum is an imperative device to comprehend the temperature and particle size dependence of the relaxation mechanism. Fig. 5.9 displays the scaling results at various temperature, i.e., the plot of normalized complex electric modulus (M''/M''_{max}) with normalized frequency $\left(f/f_{max}\right)$; where f_{max} is the frequency relating to M''_{max}. The overlapping of every curves and scaling into a solitary master curve recommends a similar relaxation process at various temperature in the present sample.

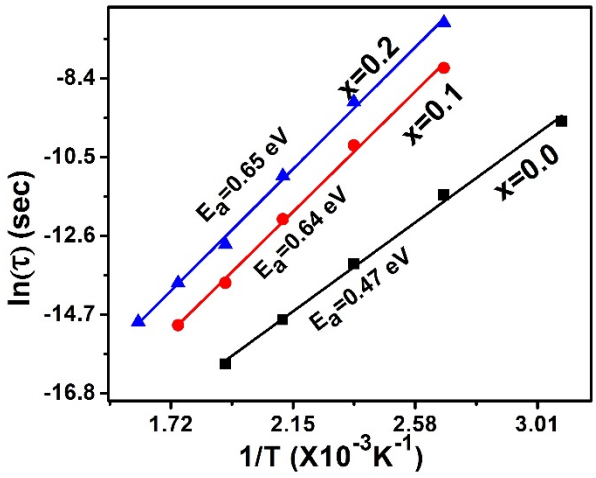

Fig. 5.10. Arrhenius plot and activation energy of CZMO with different concentration from M'' vs. f plot.

The relaxation time is estimated from the M'' vs. f plot at various temperatures and $\ln \tau$ is plotted as an element of 1/T as displayed in Fig. 5.10. It is fitted to a straight line which has exceptionally well concurrence with the Arrhenius equation. The slant of the straight line gives the activation energy, is recorded in Table 5.1. The assessed estimations of activation energy exceptionally well matched with the activation energy evaluated from Z'' vs. f plots.

Table 5.1. Activation energy calculated from different Arrhenius plots of doped Co-Zn ferrite samples.

Mo concentration (x)	E_a (eV) from Z" vs f plot	E_a (eV) from M" vs f plot
0.0	**0.52**	**0.47**
0.1	**0.65**	**0.64**
0.2	**0.66**	**0.65**